Michael G. Grotenhuis, Xiangqian Wu, Larry Flynn, Eric Beach, Jianguo Niu, and Wei Yu, " Post-launch performance evaluation of the OMPS Nadir Mapper and Nadir Profiler," Earth Observing Systems XIX, Proc. SPIE 9218, 92181V (2014).

http://dx.doi.org/10.1117/12.2062204

Post-launch performance evaluation of the OMPS Nadir Mapper and Nadir Profiler

Michael G. Grotenhuis*[a], Xiangqian Wu[b], Larry Flynn[b], Eric Beach[c], Jianguo Niu[d], Wei Yu[e]
[a]ERT, Inc. @ NOAA/NESDIS/STAR, 5830 University Research Court, College Park, MD, USA 20740; [b] NOAA/NESDIS/STAR, 5830 University Research Court, College Park, MD, USA 20740; [c]IMSG, Inc. @ NOAA/NESDIS/STAR, 5830 University Research Court, College Park, MD, USA 20740; [d]SRG @ NOAA/NESDIS/STAR, 5830 University Research Court, College Park, MD, USA 20740; [e]IMSG, Inc. @ NOAA/NESDIS/OSD, 4231 Suitland Road, Suitland, MD, USA 20746

ABSTRACT

The Joint Polar Satellite System (JPSS) represents the latest generation of polar-orbiting satellites operated by the National Oceanic and Atmospheric Administration (NOAA). The first in the JPSS series of satellites, the Suomi National Polar-orbiting Partnership (NPP) spacecraft was launched in November 2011 to bridge the gap between the current Polar Operational Environmental Satellites (POES) and the future JPSS-1. The Ozone Mapping Profiler Suite (OMPS) is a suite of hyperspectral instruments onboard the Suomi NPP spacecraft designed to continue atmospheric ozone records through both atmospheric profiles and global distribution mapping. OMPS will also be included on the future JPSS payloads. In order to properly extend measurements from previous ozone instruments, including the Solar Backscatter Ultraviolet (SBUV) instrument on POES, proper OMPS calibration is necessary. In this study, the post-launch performance of the OMPS Nadir Mapper (NM) and Nadir Profiler (NP) are evaluated through their Sensor Data Records (SDRs), which validates their end-to-end calibration. This is achieved through stability monitoring and inter-comparison.

Keywords: OMPS, JPSS, Suomi-NPP, SDR, inter-comparison, vicarious calibration, end-to-end calibration, post-launch performance

1. INTRODUCTION

The Joint Polar Satellite System (JPSS) is a collaboration between the National Oceanic and Atmospheric Administration (NOAA) and the National Aeronautics and Space Administration (NASA), and replaces NOAA's Polar Orbiting Environmental Satellite (POES) system and NASA's Earth Observing System (EOS) of satellites. Utilizing payloads of advanced Earth-observing instruments, JPSS provides critical weather, environmental, and climate data. These data provide operational continuity and enhancement from previous polar-orbiting missions for short-term weather forecasts and information on environmental hazards like hurricanes. Additionally, they extend climate data records (CDRs) and introduce new technology that will advance our climatological understanding.

The Suomi National Polar-orbiting Partnership (Suomi-NPP) spacecraft is the first in the JPSS series. Launched in October 2011, it now follows a sun-synchronous polar orbit, making approximately 14 orbits per day from a nominal equatorial altitude of 829 kilometers[1]. The Ozone Mapping Profiler Suite (OMPS) is part of the Suomi-NPP payload and consists of three ozone-measuring instruments: the Nadir Mapper (NM), also called the Total Column (TC); the Nadir Profiler (NP); and the Limb Profiler (LP). This paper will address the OMPS Nadir System, which includes both the NM and NP hyperspectral instruments. The NP takes repeated along-track measurements from a single cross-track instantaneous field of view (IFOV) with a ground resolution of 250 x 250 km. Spectrally, NP measurements cover the range from 250 to 310 nm in 147 channels. The NM measurements are acquired via 35 cross-track IFOVs, with a total swath width of 2800 km and a nadir IFOV size of 50 x 50 km. These cover the spectral range from 300 to 380 nm in 196 channels. For more detailed information on OMPS, refer to Pan et. al.[2]

*Michael.Grotenhuis@noaa.gov; phone 1 301 683-3603; fax 1 301 683-3616

To measure its radiometric degradation, the OMPS Nadir System utilizes two solar diffusers which diffuse and reflect solar light onto the NM and NP focal plane arrays (FPAs). The working diffuser is used every two weeks. However, solar diffusers are known to degrade[3], and for this reason, every six months the solar measurements are made using the reference diffuser. Since it is deployed only rarely, it is assumed that the degradation rate for the reference diffuser is much less than that of the working diffuser. Thus, long-term NM and NP radiometric trends can be maintained.

Even when Earth-observing instruments include on-board calibration devices, it is considered good practice to validate their performance by using "vicarious" sources. This confirms the accuracy of the calibration, but may also identify sources of error. Additionally, validation techniques may highlight intricacies that are not obvious using the on-board system. In a worst-case scenario, failure of the on-board calibration may require that a vicarious method take its place.

In this paper, four different methods are used to validate the OMPS Nadir System on-orbit radiometric calibration: 1) A desert in Libya is used to trend the radiometric stability of the NM over time, 2) The mean global reflectance is used to trend the radiometric stability of the NM and NP over time, 3) The Tropical Pacific is used to trend the NM radiometric stability over time and to analyze the cross-track radiometric calibration differences of the NM, and 4) "Chasing Orbits" are used to compare the NM and NP radiometric calibration to the Solar Backscatter Ultraviolet Radiometer Version 2 (SBUV/2) onboard the NOAA-19 satellite. All of the methods consider OMPS data at the calibrated instrument response, or Sensor Data Record (SDR), level.

2. OMPS NM AND NP VALIDATION METHODS AND RESULTS

2.1 Libya Desert

Deserts are popular locations to measure instrument radiometric stability, as they are generally stable over time and remain spatially homogeneous. Using them for the OMPS NM, however, offers a somewhat unique challenge in that its IFOV, or "spatial footprint", of 50 x 50 km at nadir is considerably larger than most satellite imaging systems. It is not enough that the geographical extent of the site encompass the NM IFOV; it must be significantly larger so as to generate an adequate sample size.

One desert in Libya, denoted "Libya-4", has demonstrated the necessary characteristics for radiometric trending over an area of approximately 100 x 100 km[4], and therefore it was selected to validate the NM calibration for several view angles. Due to the NP IFOV size of 250 x 250 km, only the NM was studied using Libya-4.

2.1.1 Methodology

OMPS NM data from April 1st, 2012 to June 8, 2014 from all spectral channels were collected from several view angles when the center of the IFOV was inside the collection area for Libya-4, from 27.9716 to 29.7684 degrees North latitude and 22.9642 to 25.0158 degrees East longitude. The collection area was selected to be larger than typically used for Libya-4, with the understanding that distance-from-center filtering would probably be necessary later.

The NM has 35 cross-track view angles. Libya desert data were collected for view angle #0 (westernmost), #8, #12, #17 (nadir), #26, and #34 (easternmost) in the daytime only. Because of the Suomi-NPP sun-synchronous orbit, orbital tracks have geographic regions of high density as well as other regions with low density. Thus, the collected data size differed by view angle, as did the general locations of the collected data. The number of collected data points for each view angle was 262, 300, 171, 203, 172, and 178, respectively.

The Libya Desert trending has been performed using reflectance, instead of radiance, so as to reduce effects due to differing solar illumination. Reflectance is calculated as

$$\mathrm{A} = \frac{Rd^2\pi}{\cos(\theta_S)F} \tag{1}$$

where R is the calibrated spectral radiance in milliwatts per square meter per nanometer per steradian, d is the Earth-Sun distance in astronomical units, θ_S is the solar zenith angle in radians, and F is the solar flux in milliwatts per square meter per nanometer. While using reflectance does reduce solar illumination effects, it certainly does not

eliminate them, especially considering that there is significant Rayleigh scattering in the ultraviolet, which has strong dependence on view, solar, and scattering angles.

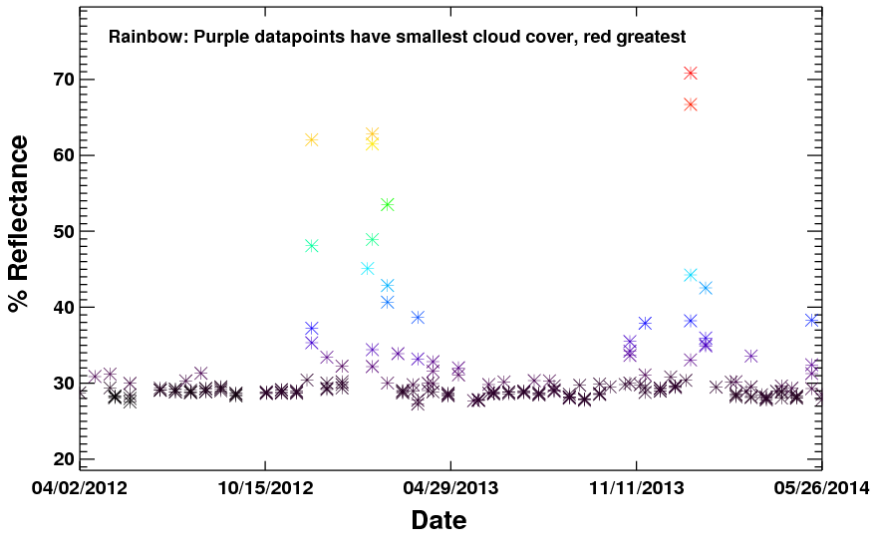

Figure 1. OMPS NM view angle #17 (nadir) 340 nm Libya Desert reflectance data with no filtering. The color of the data points corresponds to the cloud fraction parameter obtained from OMPS EDR data, where red has the greatest cloud cover.

The reflectance data at 340 nm for the nadir (#17) view angle are shown in Figure 1. The OMPS Environmental Data Record (EDR) Intermediate Product (IP) data contain a "cloud fraction" parameter that is valid for most calibrated radiances. The color of the symbols in Figure 1 correspond to the cloud fraction parameter. The out-of-family high reflectance data clearly correspond to high cloud fractions, and thus need to be filtered out. Unfortunately, cloud fractions cannot be used directly for filtering because: 1) the generation of the cloud fraction parameter depends on a surface reflectivity value that may be biased low due to absorbing aerosols, 2) the algorithm assumes proper radiance calibration which may not be the case, and 3) the algorithm was changed in late 2012. Thus, the filtering was performed using reflectance directly, with the knowledge that the high reflectances are due to the presence of clouds. The data from the different view angles were filtered using different reflectance values, as the overall trend was biased differently in each case. This is not surprising, given that the desert is likely not Lambertian and therefore reflects differently depending on the view angle. Varying accuracy of radiance calibration with view angle may also have an effect. The reflectance data were also analyzed and filtered using their distance from the desert center, though finding an appropriate cutoff value was less clear-cut than when filtering by reflectance. All view angles were filtered using a maximum of 50 km from the desert center. After filtering, view angle #0 had 74 datapoints, #8 had 75, #17 had 52, and #26 had 23. After distance filtering only, #12 had no datapoints and #34 had only 6, so there were no results generated for these view angles.

The use of the 340 nm wavelength to trend the reflectance data was based upon the desire to avoid high ozone absorption at smaller wavelengths and high Raleigh scattering at longer wavelengths. After filtering out the nadir data with 340 nm reflectance above 31% and distance-from-desert center greater than 50 km, Figure 2 was created. This 2-D plot shows the dependence of reflectance upon date and wavelength. The overall minimum for the dataset was nearly 0% reflectance, however all data below 12% have been set to the lowest brightness so as to emphasize the seasonal dependence at longer wavelengths. The plot confirms that 340 nm is an appropriate choice, as it has high signal compared to the shorter wavelengths and less variability than the longer ones.

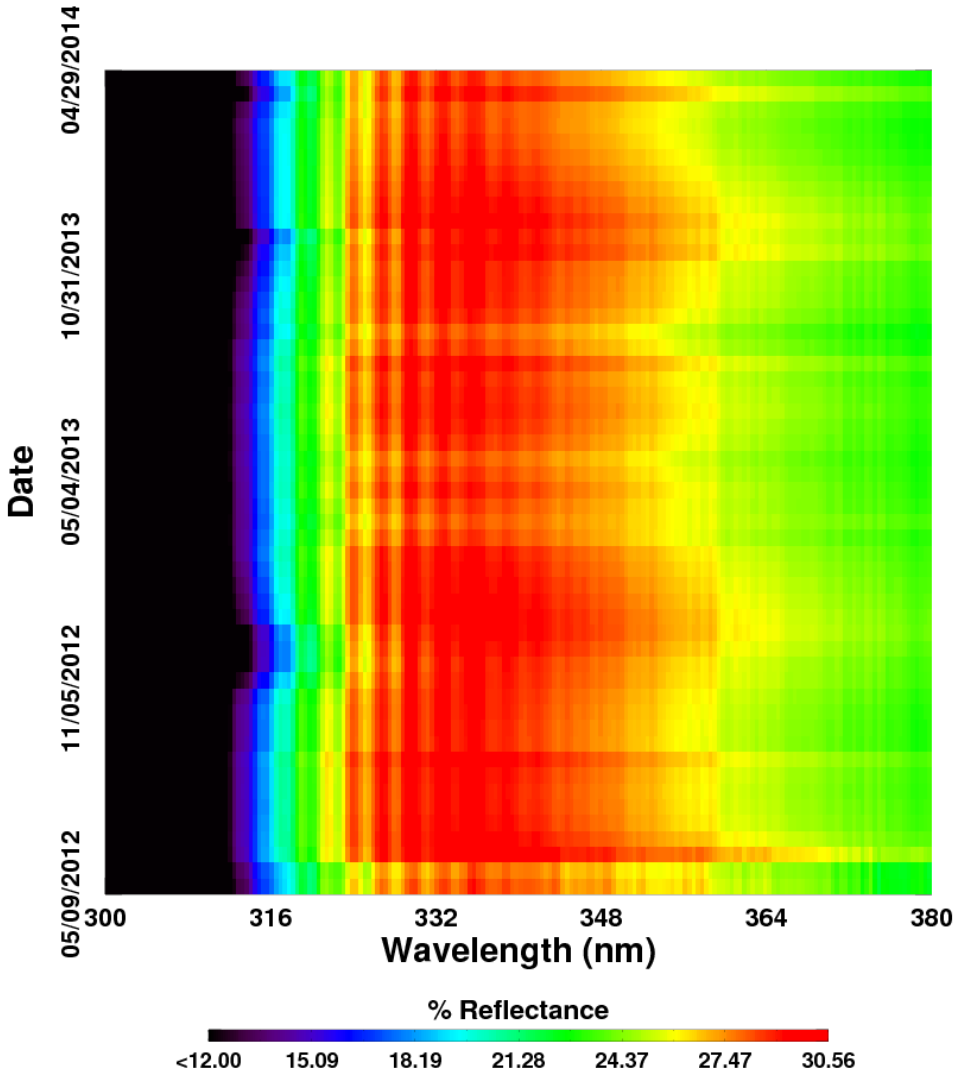

Figure 2. 2-D plot showing the dependence of the Libya Desert nadir (view angle #17) reflectance upon date and wavelength. All data below 12% reflectance, instead of the overall minimum for the dataset, are set to the lowest brightness to emphasize the variability at long wavelengths.

2.1.2 Results

Figure 3 shows the OMPS NM 340 nm reflectance trends for the #17 (nadir) view angle (left) and the #0 view angle (right). The color of the symbols in the plots corresponds to the distance from the desert center. To estimate radiometric degradation, the nadir data have been fit to a simple line:

$$R = mt + B \tag{2}$$

where t is the time in days since the first datapoint, m is the slope in reflectance per day, and B is the overall bias in reflectance. The yearly rate of degradation can be easily derived from (2):

$$D = \frac{-m*365.25}{B}*100\% \tag{3}$$

where D is the percent rate of degradation of reflectance per year. The standard deviations of the fit values m and B can be used along with propagation of error to calculate a 1-sigma uncertainty in the yearly degradation rate:

$$\sigma_D = \left|\frac{m*365.25}{B}\right| \sqrt{\left(\frac{B}{\sigma_B}\right)^2 + \left(\frac{m}{\sigma_m}\right)^2 - 2\frac{C_{mB}}{mB}} *100\% \quad (4)$$

where σ_D is the 1-sigma uncertainty estimate for the yearly degradation rate, σ_B is the standard deviation uncertainty estimate of B from the regression fit, σ_m is the standard deviation uncertainty estimate of m from the regression fit, and C_{mB} is the covariance of m and B from the regression fit.

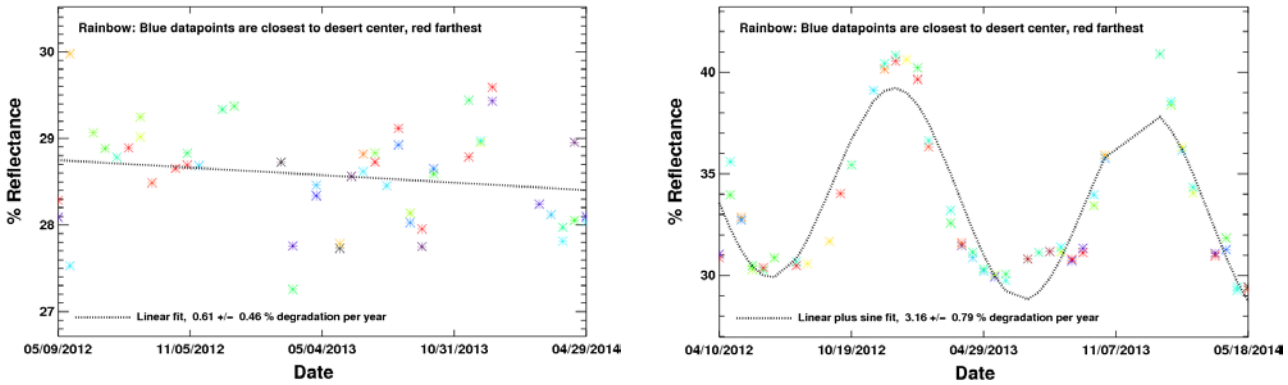

Figure 3. Libya desert OMPS NM 340 nm reflectance trends and regression fits for #17 (nadir) view angle (left), and #0 view angle (right).

The results for the #0 view angle exhibit a strong seasonal dependence. This is likely due to the bidirectional reflectance distribution function (BRDF) of the desert site and its greater sensitivity at non-nadir view angles. In future studies, we plan to implement a radiative transfer model (RTM) in an attempt to remove seasonal dependence. Alternatively, the OMPS EDR effective reflectivity could be used, which utilizes a RTM. For this study, we simply try to mitigate the dependence by adding a sine function with a period of one year to the fit:

$$\mathrm{R} = mt + B + S\sin\left(\frac{2\pi * t}{365.25} + \theta\right) \quad (5)$$

where m, t, and B are as defined in (2), S is the amplitude of the seasonal variation in reflectance, and θ is a phase angle for the seasonal dependence. Once the fit is performed, the yearly degradation and uncertainty estimate can be calculated using (3) and (4). View angle #8 also exhibited seasonal dependence. View angle #26 had too few datapoints to determine whether it had seasonal dependence, so it was regression-fit using (2).

The yearly degradation rates and one-sigma uncertainty estimates are as follows: #0, 3.16 +/- 0.79 %/year; #8: 0.58 +/- 0.91 %/year; #17 (nadir), 0.61 +/- 0.46 %/year; #26, -0.58 +/- 1.34 %/year. The negative degradation for #26 would seem to indicate an accumulation of signal over time, but should of course be interpreted in terms of its high uncertainty and small number of datapoints.

2.2 Mean Global Reflectance

An antithetic approach to selecting specific Earth targets for validation is to consider the globe as a whole. This is a concept that has been successfully applied to other remote sensing instruments[5]. However, while it may appeal intuitively, we do not know of any evidence that the Earth as a whole remains stable at the OMPS NM and NP wavelength range. In fact, there are known seasonal and long-term changes in global ozone concentration, which especially affect signals at short OMPS wavelengths (~250-340 nm). Therefore, results can only be as good as the

natural variability, and should be considered cautiously. Derived degradation rates that are similar to other methods can be interpreted as a type of validation, but dissimilar results should not be construed as invalidation.

2.2.1 Methodology

Radiances from all measurements within a solar zenith angle of 75 degrees (to limit to data with high signal-to-noise) were collected for weeklong periods, converted to reflectance, and then averaged. This was done for several wavelengths for both the NM and NP.

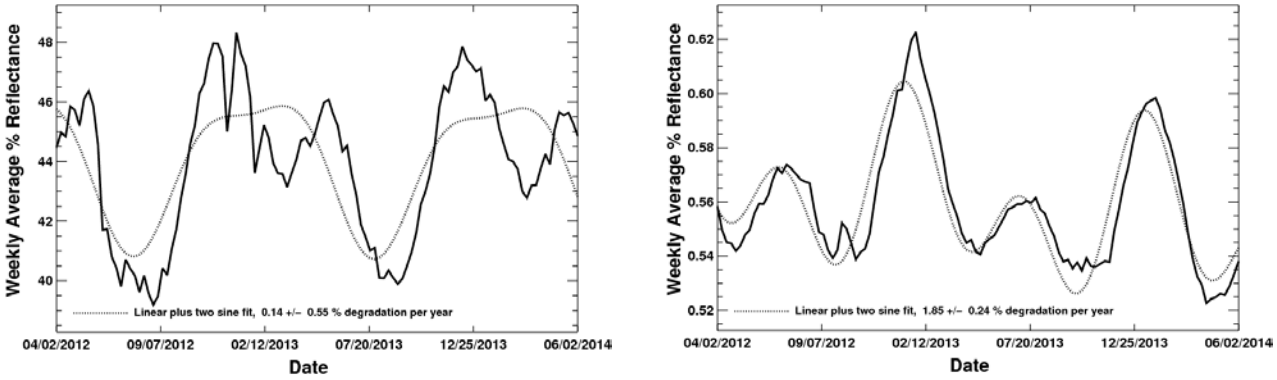

Figure 4. NM global reflectance weekly average at 360 nm (left) and NP global reflectance weekly average at 300 nm (right).

Table 1. Degradation rates and uncertainties for the NM and NP using the mean global reflectance method.

Instrument	Wavelength (nm)	View Angle	Degradation Rate and Estimated Uncertainty (% per year)*
NP	255	N/A	1.90 +/- 0.51
NP	265	N/A	0.00 +/- 0.21
NP	280	N/A	4.27 +/- 0.32
NP	300	N/A	1.85 +/- 0.24
NM	330	#17	-0.71 +/- 0.43
NM	340	#0	-0.09 +/- 0.20
NM	340	#8	-0.82 +/- 0.42
NM	340	#17	-0.30 +/- 0.47
NM	340	#26	-0.57 +/- 0.43
NM	340	#34	-1.07 +/- 0.30
NM	360	#17	0.41 +/- 0.55
NM	380	#17	-1.04 +/- 0.60

***: A negative degradation rate indicates a signal accumulation with time. All results should be interpreted in terms of their 1-sigma uncertainty estimation.**

2.2.2 Results

The left side of Figure 4 shows the results for the NM at 360 nm, and the right side shows the NP results at 300 nm. These data seem to suggest a bi-yearly seasonal dependence. This is likely due to, amongst other effects, the variation in solar zenith angle. To mitigate, the data are fit to (5) with the addition of a sine function with a period of half a year:

$$\mathrm{R} = mt + B + S_1 \sin\left(\frac{2\pi * t}{365.25} + \theta_1\right) + S_2 \sin\left(\frac{4\pi * t}{365.25} + \theta_2\right) \quad (6)$$

where m, t, and B are as defined in (2), S_1 is the amplitude of the seasonal variation in reflectance, θ_1 is a phase angle for the seasonal dependence, S_2 is the amplitude of the bi-yearly variation in reflectance, and θ_2 is a phase angle for the bi-yearly variation.

The degradation rate and uncertainty are obtained using (3) and (4). A summary of degradation rates and uncertainties for the NM and NP is provided in Table 1.

2.3 Tropical Pacific

The OMPS Nadir Mapper acquires data in cross-track swaths of 35 elements. In order to evaluate how the calibration differs cross-track, a validation location is required with a large longitudinal extent so as to generate meaningful statistics for each cross-track view angle. The Tropical Pacific (20°S–20°N, 100°W–180°W), has been used for OMPS NM trending for both Environmental Data Record (EDR)[6], and Sensor Data Record (SDR)[7], or calibrated radiance, data. This area was selected due to a low amount of aerosols, small degree of cloud cover, and homogeneous ozone amounts. The combination of these factors makes the Tropical Pacific a temporally stable Earth target at OMPS NM wavelengths (though there is some temporal variability in ozone concentration, which especially affects OMPS ozone-absorbing channels, which begin around 340 nm and become more affected toward shorter wavelengths). Also, due to its longitudinal size, it can be used to evaluate NM cross-track calibration differences.

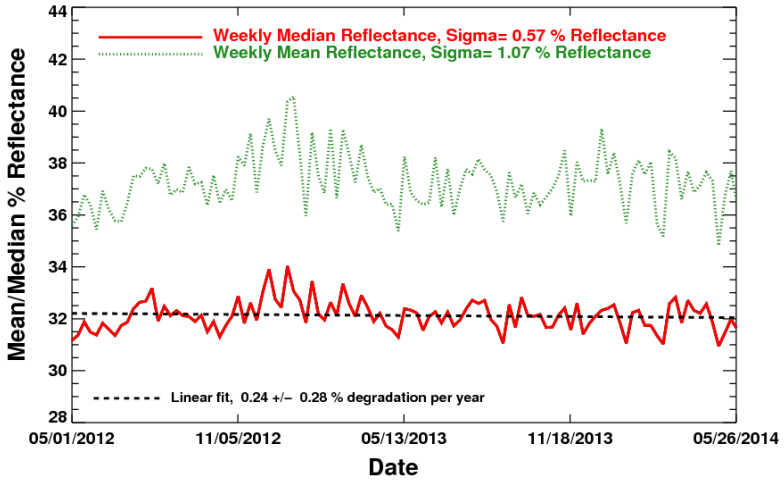

Figure 5. Tropical Pacific median and mean reflectivity over weeklong periods for OMPS NM nadir (#17) view angle at 340 nm.

2.3.1 Methodology

Both Wu et. al.[7] and Flynn et. al.[6] tracked reflectivity data over the Tropical Pacific by sorting reflectivity data acquired over a week and selecting the datapoint at the 1 percentile level, though it should be noted that Wu et. al. adjusted the reflectivity data by the secant of the solar zenith angle to account for differences in Raleigh scattering due to longer atmospheric optical path lengths. This 1 percentile level has been shown to consistently select clear dark ocean reflectivity, which is invariant in the Tropical Pacific.

An alternative is to select the median, or 50 percentile level. This is a stronger signal than the 1 percentile and, given a low incidence of clouds, may also provide stable data (though some seasonal variation in the solar illumination and sun glint are to be expected). To determine whether this is the case, data were acquired from the NM nadir pixel at 340 nm over the Tropical Pacific for weeklong periods, and the median value was selected. Figure 5 shows the result. The median value is generally stable over time, with a 1-sigma standard deviation of 0.59% reflectivity, which amounts to about 1.8% of the overall signal bias. Note that the mean value for the weeklong periods is also plotted, and exhibits greater variability. This is because the mean value is more susceptible to high reflectance clouds, which appear at infrequent intervals over the Tropical Pacific.

Because of the longitudinal extent of the Tropical Pacific area, data can be collected for all NM view angles with meaningful statistical data size and then compared to examine potential differences in the cross-track calibration accuracy. This was done for all Nadir Mapper wavelengths (300-380 nm) from May 1st, 2012 to May 26, 2014.

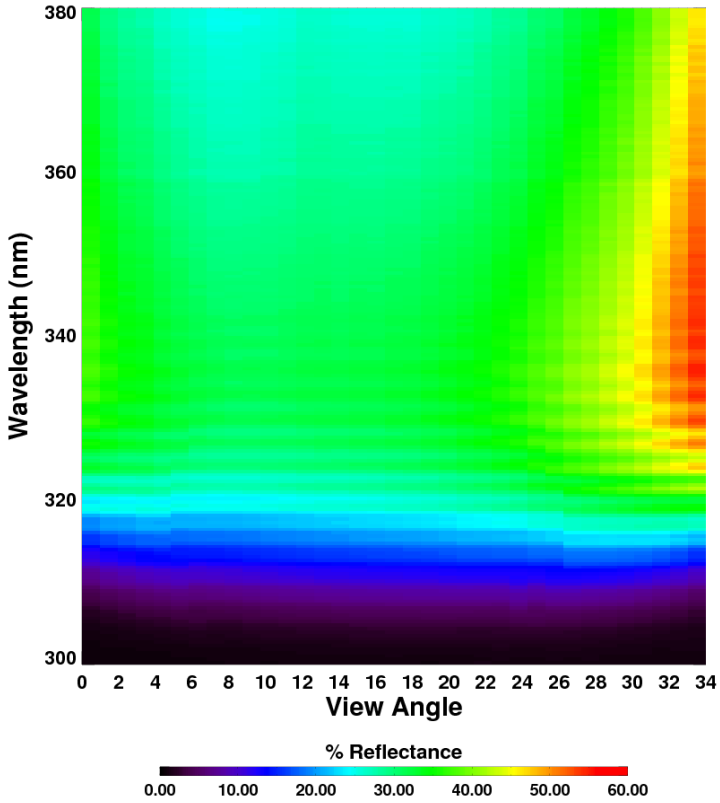

Figure 6. OMPS NM median reflectivity values over the Tropical Pacific at different wavelengths and view angles for the period from May 26 to June 1, 2014.

2.3.2 Results

The long-term stability of the median reflectance over the Tropical Pacific, necessary to measure the NM cross-track calibration accuracy, is demonstrated in Figure 5. However, the median reflectance should also be susceptible to instrument degradation, so the long-term instrument performance can also be measured as it was for the Libya Desert and mean global reflectance. Thus, the median values at 340 nm were fit to (2) and the degradation rate and estimated uncertainty were measured using (3) and (4) for three NM view positions. Figure 5 shows the linear fit for the nadir (#17) view angle. The degradation rate and uncertainty for the NM #0 (easternmost) view angle was 1.52 +/- 0.60 %/year, for the #17 (nadir) view angle was 0.24 +/- 0.28 %/year, and for the #34 (westernmost) was -0.35 +/- 0.51 %/year.

The NM Tropical Pacific median reflectivity values for all view angles and wavelengths for the week from May 26 to June 1, 2014 are displayed in Figure 6. Cross-track differences in calibration accuracy are evident in the differences in the median reflectivity values of view angles at a given wavelength. The cross-track differences also depend on wavelength. To determine whether cross-track differences are stable with time, the median values for the view angle positions at certain wavelengths were acquired on different dates. Figure 7 shows the results at 340 and 370 nm. Generally, the different dates have different overall biases, but the relative differences between view angles are similar. This was also seen in plots at 355 and 380 nm (not shown).

Overall, the data indicate that the cross-track differences are very significant. Recall, however, the finding of Wu et. al.[7] that there are differences between view angles in Raleigh scattering due to longer atmospheric optical path lengths. A BRDF effect is certainly also possible. Additionally, the consistent sun-synchronous orbital track of Suomi-NPP may

cause selection biases between view angles, so that different view angles may be acquiring data from different sections of the Tropical Pacific region.

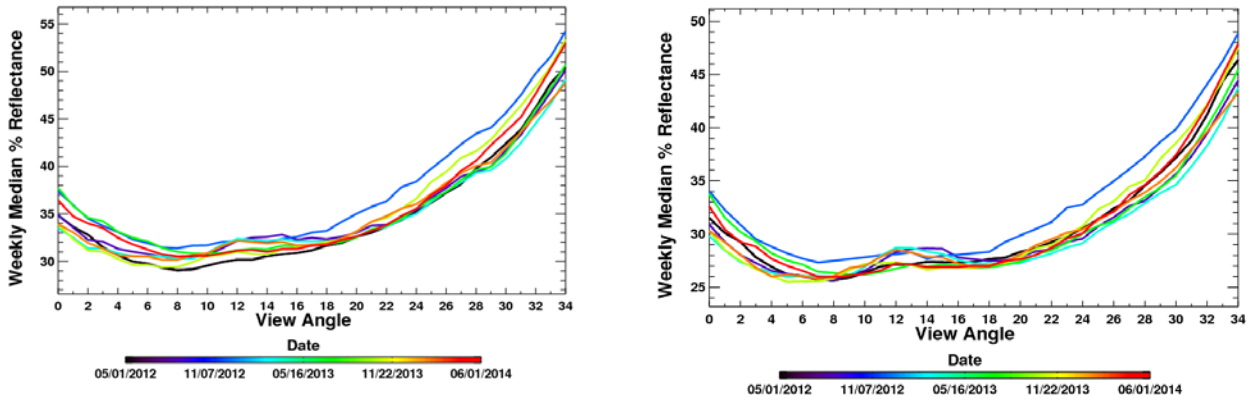

Figure 7. NM weekly median reflectivity values at 340 nm (left) and 370 nm (right) over the Tropical Pacific as a function of view angle for several dates from May 1, 2012 to June 1, 2014.

2.4 Chasing Orbit comparisons with the NOAA-19 SBUV/2

Periodically, the polar orbit of the Suomi-NPP satellite, which carries the OMPS instrument suite, and the polar orbit of the NOAA-19 spacecraft align, with a small difference in equator crossing time and location. These "chasing orbits" create an opportunity to inter-compare the OMPS NM and NP with the ozone instrument onboard NOAA-19, the Solar Backscatter Ultraviolet Instrument (SBUV/2). Unlike the previous three methods, which evaluate the relative calibration accuracy of OMPS NM/NP, the chasing orbits comparison evaluates the absolute calibration performance. It should be noted, however, that the performance of the SBUV/2 instrument was not evaluated in this study.

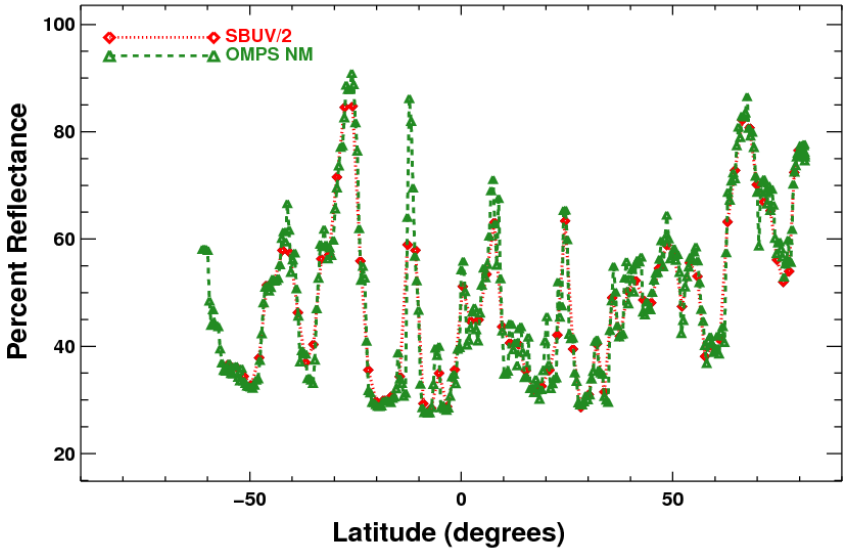

Figure 8. OMPS NM and SBUV/2 reflectances at 343 nm for the chasing orbit on May 24, 2014.

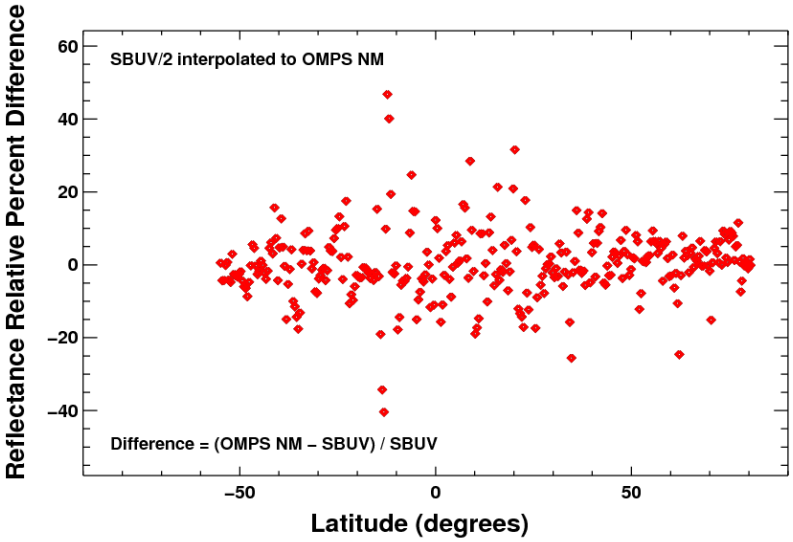

Figure 9. OMPS NM and SBUV/2 relative differences at 343 nm for the chasing orbit on May 24, 2014.

2.4.1 Methodology

For this comparison, Suomi-NPP and NOAA-19 are considered to have "chasing orbits" when the difference between their Equator crossing time is less than 30 minutes and the longitudinal difference at the Equator crossing is less than 0.05 degrees. Thirty-nine chasing orbits have been detected since January 28, 2012.

The SBUV/2 measurements from its 12 different channels are acquired sequentially, not simultaneously. An acquisition sequence starts with a 0.75 second delay, then a channel 1 measurement is made with a 1.25 second integration, then there is another 0.75 second delay followed by a channel 2 measurement, and so on. After the channel 12 measurement, there is an 8 second delay before the sequence starts again. However, the spacecraft latitude, longitude, and solar zenith angle are only provided at the start of the sequence. Therefore, they must be interpolated given their begin-scan values and the acquisition sequence timing to determine their values for a given channel's measurement. The interpolation was performed linearly.

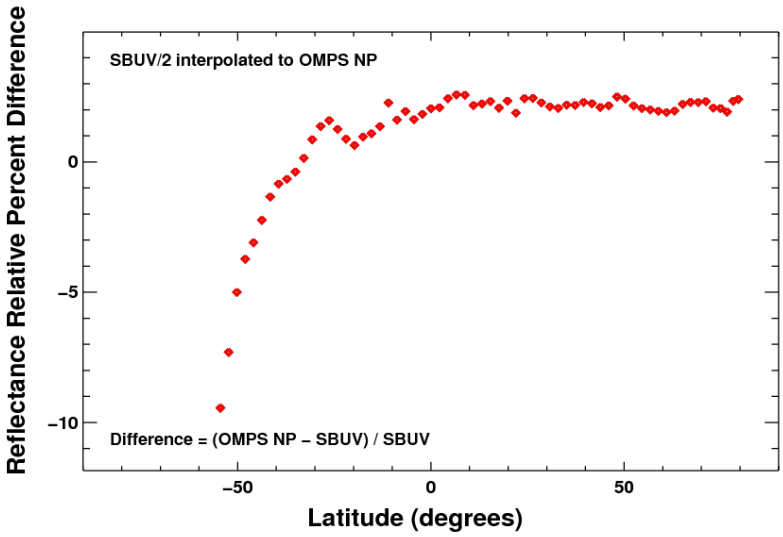

Figure 10. OMPS NP and SBUV/2 relative differences at 292 nm for the chasing orbit on May 24, 2014.

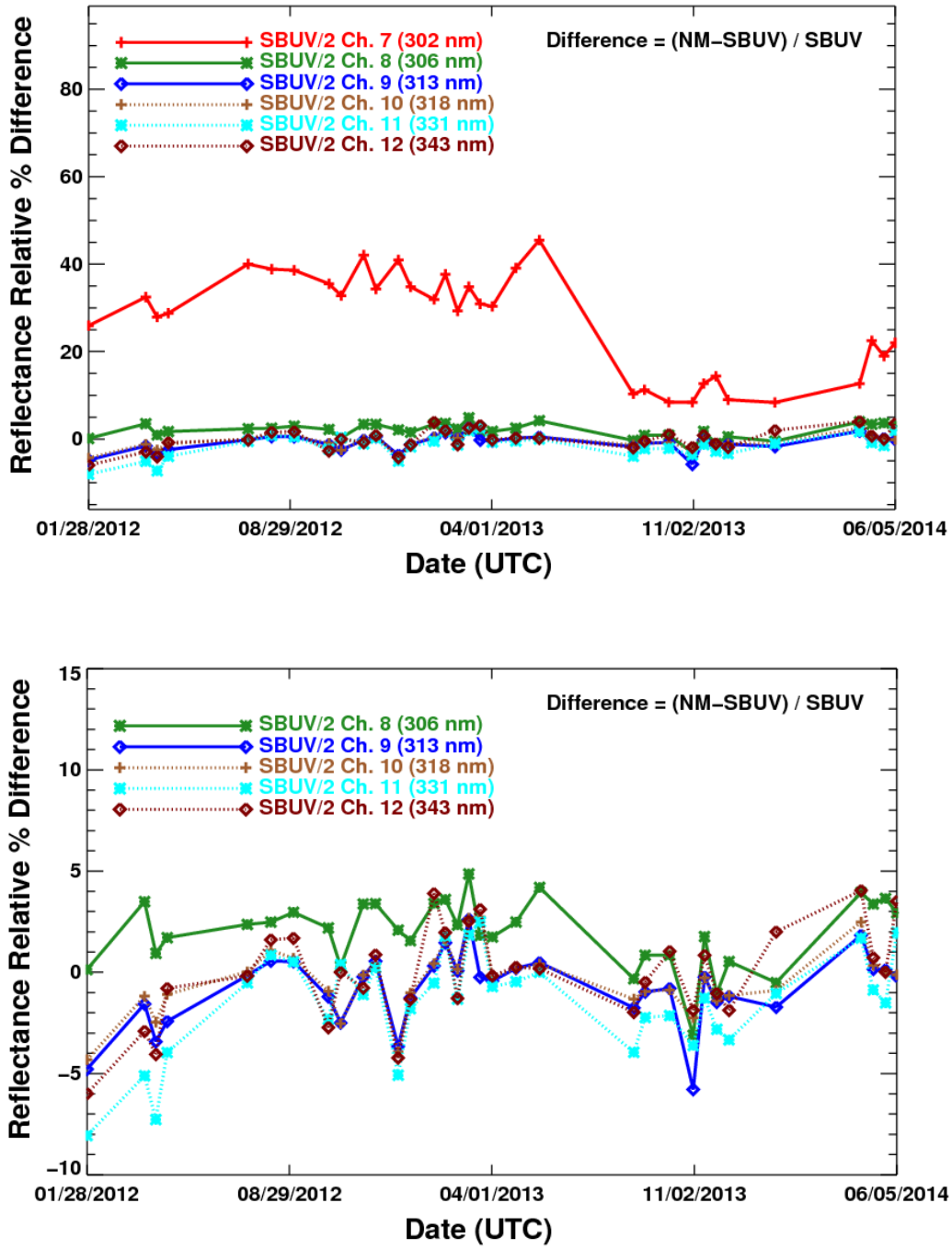

Figure 11. OMPS NM-SBUV/2 chasing orbit long-term relative differences using zonal average showing all channels (top) and SBUV channels 8-12 (bottom).

The SBUV/2 instrument takes measurements in calibrated "N-Values":

$$\mathrm{N} = -100\log(I/F) \tag{7}$$

where I is the Earth spectral radiance and F is the solar flux. These "N-Values", taken at 12 wavelengths from 252 to 340 nm, can easily be converted into reflectance so as to compare with OMPS:

$$\mathrm{A_{SBUV/2}} = \frac{\pi 10^{(N/-100)}}{\cos(\theta_{S-SBUV/2})} \tag{8}$$

where $\theta_{S-SBUV/2}$ is the solar zenith angle of the SBUV/2 Earth measurement.

The SBUV/2 spatial footprint is about 7.5 km along-track and 160 km cross-track. Because of the sequential acquisition sequence of the SBUV/2, neighboring measurements from a given channel cannot be combined to increase the along-track footprint size. Thus, when comparing the SBUV/2 to the OMPS NM/NP, the along track spatial differences are significant, as the OMPS NM nadir pixel is about 50 x 50 km and the NP is about 250x 250 km. In the cross-track direction, the OMPS NM nadir and two neighboring pixels can be averaged to better match the SBUV/2. There are not multiple SBUV/2 measurements in the cross-track direction.

To directly compare the SBUV/2 data to the OMPS NM/NP, the SBUV/2 measurements are linearly interpolated so that their latitudes match those of the OMPS NM and NP.

2.4.2 Results

OMPS NM and SBUV/2 reflectance values at 343 nm for the chasing orbit on May 24, 2014 are shown in Figure 8. Qualitatively, the measurements between the two instruments appear to match well. For better comparison, the relative difference in the measurements can be calculated, as shown in Figure 9. Relative differences are calculated as the difference between an OMPS and a SBUV/2 reflectance value, divided by the SBUV/2 value. Figure 9 shows that the relative differences are mostly within 10%, and nearly completely within 20%. This is typical for NM-SBUV/2 chasing orbit comparisons at 306, 313, 318, 331, and 343 nm. Comparisons at 302 nm show very large differences, sometimes as large as 60%. These are thought to be due to NM stray light contamination, which will soon be corrected within the ground software.

The relative differences between the NP and SBUV/2 at 292 nm for the chasing orbit on May 24, 2014 are displayed in Figure 10. The "tail" at extreme Southern latitudes is typical for all chasing orbits and NP wavelengths. An investigation is needed to determine its cause. It is not believed to be due to spatial mismatch, as the OMPS NM shows no such feature. However, the NP may be especially affected by atmospheric variability and solar zenith angle changes, which are greater at higher latitudes. Even including the "tail", relative differences are within 10% for NP-SBUV/2 chasing orbit comparisons at 252, 274, 283, 288, 292, 298, and 306 nm. Relative differences are larger at 302 nm, but are usually within about 15%. These larger differences may be due to NP stray light contamination (though this has been measured to be small at 302 and 306 nm) as well as a shift in the dichroic filter, which affects the wavelength registration. Fixes for these will be implemented soon.

To examine any long-term changes in NM/NP absolute calibration accuracy, a zonal average was used. The location of the minimum solar zenith angle was determined for each chasing orbit, and the mean reflectance within 10 degrees was calculated for both OMPS and the SBUV/2 (the purpose for using the zonal mean around the minimum solar zenith angle was to avoid potential seasonal effects). The relative difference between these averages was then calculated for each chasing orbit. Figure 11 shows the result for the NM. The high error at 302 nm is evident, though it drops significantly after June 3rd, 2013. This coincides with a NM stray light calibration table update, which especially affects wavelengths near 300 nm. Otherwise, there appears to be no long-term trend, and the relative differences are within 5%.

A similar plot for the NP is displayed in Figure 12. The 252 nm trend is greater than 10% until February 24, 2013, when it decreases significantly. This is due to the implementation of NP dark current calibration tables that improved radiometric accuracy particularly for shorter wavelength channels. The higher error at 302 nm is also evident. Additionally, the data prior to August 8, 2012 exhibit behavior unlike the rest of the trend, as they occurred prior to a

change in the solar flux values within the SDR data. Otherwise, there is no apparent long-term trend, with errors mostly within 5%.

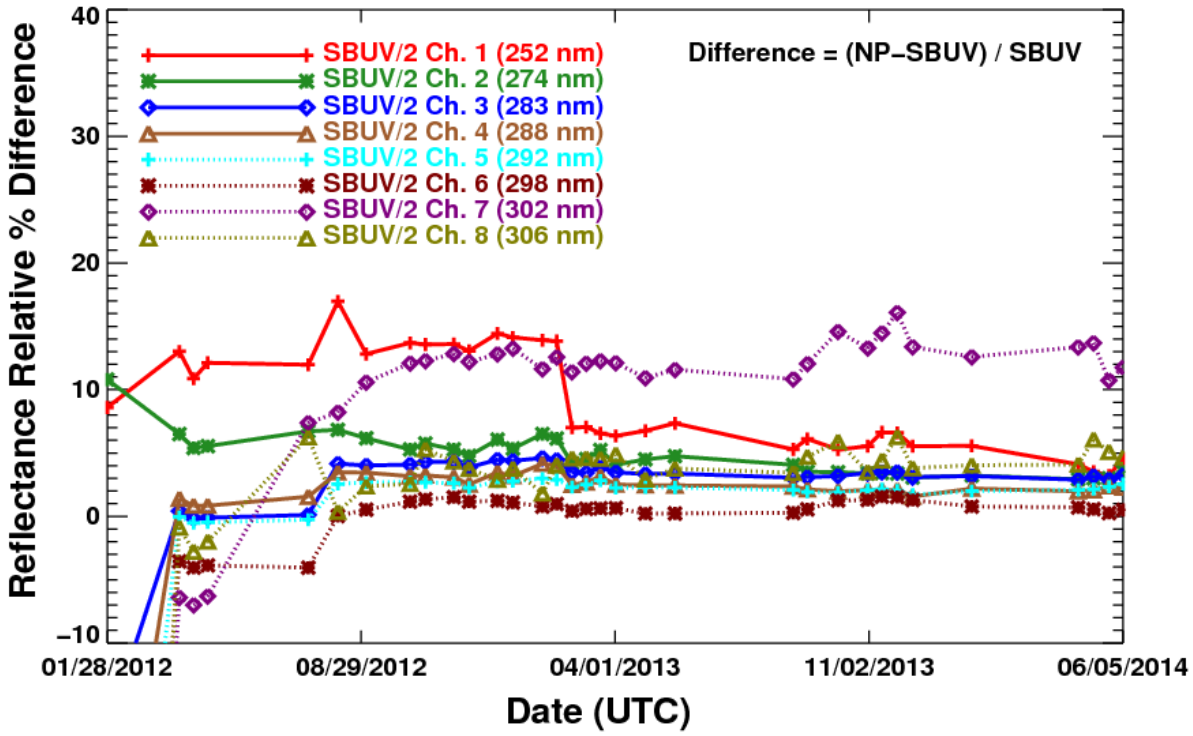

Figure 12. OMPS NP-SBUV/2 chasing orbit long-term relative differences using zonal average.

3. SUMMARY OF RESULTS AND DISCUSSION

A summary of the radiometric trending results for the Libya Desert, mean global reflectance, and Tropical Pacific methods are listed in Table 2. It should be noted that, while radiometric degradation is expected to occur to the instrument as a whole, it is not unreasonable to expect some difference depending on wavelength and view angle. Even disregarding that expectation, however, the results seem to agree well, with nearly all within 3 standard deviations of each other. For the NM, there is one exception: the Libya Desert reflectance at 340 nm and view angle 0. The raw data for this trend did exhibit a strong sinusoidal seasonal variation, so it would likely benefit from the utilization of a radiative transfer model. Overall, the data suggest a low rate of degradation, probably between 0 and 1% per year.

For the NP, there is only global reflectance data available. The results do not agree as well as those for the NM. Considering the potential issues with using global reflectance data, including strong seasonal variation and significant long-term trends in global ozone, especially at the NP wavelengths, the lack of cohesion in the results is not surprising.

The NM differences in cross-track calibration accuracy depend upon wavelength and are significant, though care should be taken when interpreting the results, given, among other things, a known difference in the solar zenith angle, and therefore Raleigh scattering, with view angle.

Finally, inter-comparisons with the SBUV/2 show relative differences usually within 10% for the NM and 5% for the NP. The largest errors are believed to be due to stray light contamination for both the NM and NP and a shift in the dichroic filter for the NP, causing wavelength registration issues. Corrections made using the ground software are expected to be implemented soon. Plots for all SBUV/2 – OMPS NM/NP chasing orbit comparisons are available at the NOAA Center for Satellite Applications and Research (STAR) Integrated Calibration/Validation System (ICVS) website.

Table 2. Summary of radiometric trending results for the Libya-4 Desert, mean global reflectance, and Tropical Pacific methods.

Instrument	Method	Wavelength (nm)	View Angle	Degradation Rate and Estimated Uncertainty (% per year)*
NM	Libya-4	340	0	3.16 +/- 0.79
		340	8	0.58 +/- 0.91
		340	17 (nadir)	0.61 +/- 0.46
		340	26	-0.58 +/- 1.34
	Global	330	17 (nadir)	-0.71 +/- 0.43
		340	0	-0.09 +/- 0.20
		340	8	-0.82 +/- 0.42
		340	17 (nadir)	-0.32 +/- 0.54
		340	26	-0.57 +/- 0.43
		340	34	-1.07 +/- 0.30
		360	17 (nadir)	0.41 +/- 0.55
		380	17 (nadir)	-1.04 +/- 0.60
	Pacific	340	0	1.52 +/- 0.60
		340	17 (nadir)	0.24 +/- 0.28
		340	34	0.35 +/- 0.51
NP	Global	255	N/A	1.90 +/- 0.51
		265	N/A	0.00 +/- 0.21
		280	N/A	4.27 +/- 0.32
		300	N/A	1.85 +/- 0.24

***: A negative degradation rate indicates a signal accumulation with time. All results should be interpreted in terms of their 1-sigma uncertainty estimation.**

ACKNOWLEDGEMENTS

The authors thank Fangfang Yu for her assistance in selecting the Libya-4 desert site. This work is funded by the NOAA/NESDIS/STAR Calibration/Validation support. The contents of this document are solely the opinions of the authors and do not constitute a statement of policy, decision, or position on behalf of NOAA or the U.S. government.

REFERENCES

[1] Cao, C., De Luccia, F. J., Xiong, X., Wolfe, R. and Weng, F., "Early on-orbit performance of the Visible Infrared Imaging Radiometer Suite onboard the Suomi National Polar-orbiting Partnership (S-NPP) satellite," IEEE Transactions on Geoscience and Remote Sensing 52(2), 1142-1156 (2014).

[2] Pan, C., Kowalewski, M., Buss, R., Flynn, L., Wu, X., Caponi, M. and Weng, F., "Performance and calibration of the Nadir Suomi-NPP Ozone Mapping Profiler Suite from early-orbit images," IEEE Journal of Selected Topics in Applied Earth Observations and Remote Sensing 6(3), 1539-1551 (2013).

[3] Xiong, X. and Barnes, W., "An overview of MODIS radiometric calibration and characterization," Advances in Atmospheric Sciences 23(1), 69-79 (2006).

[4] Henry, P., Lachérade, S., Fougnie, B. and Lafrance, B., "General characteristics of LIBYA-4," CEOS-IVOS Libya-4 Workshop (2012).

[5] Stone, T. C., Rossow, B., Ferrier, J. and Hinkelman, L., "Lunar calibration applied to geostationary imagers of the ISCCP dataset," Proc. CALCON Technical Conference (2011).

[6] Flynn, L., Long, C., Wu, X., Evans, R., Beck, C. T., Petropavlovskikh, I., McConville, G., Yu, W., Zhang, Z., Niu, J., Beach, E., Hao, Y., Pan, C., Sen, B., Novicki, M., Zhou, S. and Seftor, C., "Performance of the Ozone Mapping and Profiler Suite (OMPS) products," J. Geophys. Res. Atmos. 119, 6181-6195 (2014).

[7] Wu, X., Liu, Q., Zeng, J., Grotenhuis, M., Qian, H., Caponi, M., Flynn, L., Jaross, G., Sen, B., Buss, R. H., Johnsen, W., Janz, S., Pan, C., Niu, J., Beck, T., Beach, E., Yu, W., Varma Raja, R., Stuhmer, D., Cumpton, D., Owen, C. and Li, W., "Evaluation of the Sensor Data Record from the nadir instruments of the Ozone Mapping Profiler Suite (OMPS)," J. Geophys. Res. Atmos. 119, 6170–6180 (2014).